Infrared Spectra of Dialanes in Solid Hydrogen

Lester Andrews* and Xuefeng Wang

Department of Chemistry, P.O. Box 400319, University of Virginia, Charlottesville, Virginia 22904-4319

Received: December 10, 2003; In Final Form: February 25, 2004

Laser-ablated Al atoms react with H_2 during co-deposition at 3.5 K to produce AlH and smaller amounts of AlH_2 and AlH_3. Ultraviolet irradiations markedly increase the yields of AlH_2 and particularly AlH_3, which is characterized as the hypervalent $(H_2)AlH_3$ complex in solid hydrogen. Simultaneous annealing to 5−6 K with concurrent photolysis allows a 4-fold increase in Al_2H_6 absorption intensities. New absorptions are assigned to the Al_2H_5 radical with the dibridged structure. A neon overcoat extends the annealing range for solid hydrogen and facilitates the observation of trialane Al_3H_9. The AlH_4^- and AlH_3^-[AlD_4^-, AlD_3^-, and AlD_2^-] anions and $Al^+(H_2)_n[Al^+(D_2)_n]$ cations are observed in solid hydrogen [deuterium] and in solid neon. Dialane is prepared in solid neon with dilute Al and H_2 on $\lambda > 240$ nm irradiation and not on annealing, which suggests activation energy for the alane dimerization reaction.

Introduction

The first successful synthesis of dialane, Al_2H_6, was reported from this laboratory using laser-ablated aluminum with pure hydrogen as the reagent and matrix.[1] The lower dialuminum species Al_2H_4 was also observed in these samples from both laser-ablated Al atoms and thermal Al atoms.[2] Since the above dialuminum species result from dimerization of AlH_3 and AlH_2, the Al_2H_5 radical can also be formed, and the infrared spectrum of the dibridged Al_2H_5 radical is reported here. It appears that Al_2 reacts spontaneously with H_2 to form Al_2H_2.[2] In this investigation we have increased the dialane band intensities by a factor of 4 over our earlier experiments,[1,2] which makes possible the observation of another Al_2D_6 fundamental. We have also found evidence for higher alanes, which have been the subject of earlier calculations.[3,4]

In a very recent highlight review of the group 13 binary hydrides, Mitzel concluded with several questions remaining to be answered, including the possible existence of hypervalent AlH_5.[5] We report here evidence for the $(H_2)AlH_3$ complex, which involves a weak 3-center-2-electron bond.

The tetrahydroaluminate, AlH_4^-, anion is a well-known reducing agent,[6] and it is also observed in irradiated Al/H_2 samples and laser-ablation experiments where electrons are produced.[2,7] These experiments also provided the first experimental evidence for the lower oxidation state AlD_2^- anion. Here, we examine the ultraviolet photochemical conversion of AlD_2^- in solid D_2 to AlD_4^- and the mechanism of formation for AlH_4^-. Finally, the electron affinity calculated for AlH_3 (10 kcal/mol)[2] suggests that AlH_3^- has some stability and might be observable.[8]

Experimental and Theoretical Methods

The combined laser-ablation matrix-isolation experiment with normal hydrogen (2−3 mmol) has been described previously.[9,10] We focus a 10−40 mJ per 10 ns pulse of 1064 nm radiation onto a rotating aluminum target. To extend the annealing range of solid hydrogen, we have applied a neon overcoat (1 mmol), which appears to work better for hydrogen than an argon overcoat.[11] We have warmed the sample using resistance heat and extended the irradiation farther into the ultraviolet with 193 nm ArF laser (Optex, 2−6 mJ/pulse) and into the infrared with external Nernst glower sources. Laser-ablation plume emission spectra were recorded using an Ocean Optics optical fiber spectrometer.

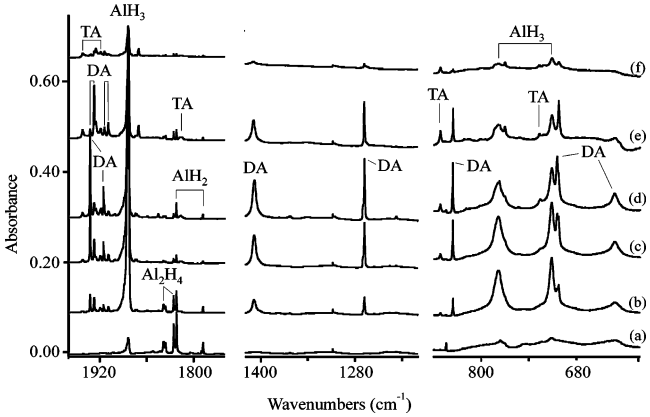

Figure 1. Infrared spectra in selected regions for laser-ablated Al using 40 mJ/pulse co-deposited with normal hydrogen at 3.5 K. (a) Spectrum of deposited sample, (b) after $\lambda > 240$ nm irradiation at 5.4 K for 20 min, (c) after $\lambda > 240$ nm irradiation at 5.7 K for 50 min, (d) after Nernst glower irradiation at 5.3 K for 30 min, (e) after annealing to 7.0 K, and (f) after annealing to 8.0 K.

Additional density functional theory (DFT) calculations of aluminum hydride radicals were done for comparison with experimental values using the Gaussian 98 system as described in our earlier reports.[1,2]

Results and Discussion

New aluminum−hydrogen experiments will be described and the alane and charged hydride species formed will be identified.

Al_2H_6 System. Laser-ablated Al atoms were co-deposited with pure normal hydrogen, and the samples were extensively irradiated and annealed to increase the product yield. Figure 1 illustrates the highest yield of dialane we were able to obtain in several attempts: trace (a) illustrates the initial deposited sample: a neon overcoat had no effect on this spectrum. Full arc ($\lambda > 240$ nm) photolysis was done stepwise with the sample

10.1021/jp037792e CCC: $27.50
Published on Web 04/16/2004

TABLE 1: Comparison of Calculated and Observed Frequencies (cm^{-1}) for Dialane Al_2H_6 and Al_2D_6

B3LYP/6-311++G(d,p)[a]		observed[b]	
H	D	H	D
1989 (419) b_{1u}	1446 (242)	1932.3 (1927.2 site)	1415.0
1966 (126) b_{3u}	1398 (91)	1915.1 (1909.1 site)	c
1483 (1096) b_{3u}	1066 (603)	1408.1	1036.2 (1031.6, 1028.5 sites)
1292 (352) b_{2u}	937 (205)	1268.2	931.6 (925.2, 919.9 sites)
866 (244) b_{1u}	625 (124)	835.6	607.5
712 (648) b_{3u}	517 (330)	702.4 (704.4 site)	510.6
634 (263) b_{2u}	459 (133)	631.9	459.1 (462.4 site)
223 (13) b_{1u}	158 (6)		

[a] This work. Intensities, km/mol, in parentheses. D_{2h} structure, refs 2, 17, 18. [b] This work: solid normal H_2 and solid D_2. [c] Mode predicted to lie under strong AlD_3 absorption.

TABLE 2: Comparison of Calculated and Observed Frequencies (cm^{-1}) for the Dibridged Al_2H_5 Radical

calculated[a]	observed[b]	identification
1970	1918[c]	terminal Al−H_2
1887	1845[c]	terminal Al−H
1422	1363[c]	Al−H−Al bridge
1345	1307	Al−H−Al bridge, a″
1261	1228	Al−H−Al bridge, a″
806	753	Al−H_2 bending

[a] B3LYP/6-311G(d,p). [b] Solid hydrogen, this work. [c] Al_2D_5 counterparts at 1403, 1354, and 992 cm^{-1}, respectively, in solid D_2.

held at 5.4 K, and the spectrum was recorded after 20 min is shown in Figure 1b; the Al_2H_4, AlH_2, and AlH (not shown) absorptions are reduced markedly, and three very strong AlH_3 and seven strong Al_2H_6 (labeled DA) bands are produced, as reported previously.[1,2,12−16] The two site split terminal Al−H_2 fundamentals (1932.3, 1927.2 and 1915.1, 1909.1 cm^{-1}), two bridge stretching Al−H−Al modes (1408.1 and 1268.2 cm^{-1}), and three bending vibration bands (835.6, 702.4, 631.9 cm^{-1}) are labeled DA in the figure[1,2,17,18] and listed in Table 1. The 702.4 cm^{-1} fundamental also shows a 704.4 cm^{-1} site splitting. An additional full arc irradiation with the sample at 5.4−5.7 K over a 50 min period produced the spectrum in Figure 1c and a 2.2 factor growth in the DA bands. Infrared radiation from an external glower source for 60 min with the sample at 5.4 K, Figure 1d, resulted in another 25% growth for the seven DA bands in concert. Additional weaker bands are observed at 851.5, 770.2, 752.8, and 726.7 cm^{-1} in the lower region, at 1362.8, 1306.6, and 1227.8 cm^{-1} in the bridge stretching and at 1942.0, 1925, 1919.6, 1918.3, 1914, 1873.2, 1871, 1845.1, and 1816.7 cm^{-1} in the upper region. A further 30 min full arc photolysis produced no changes in the spectrum. Next, annealing to 7 K, a temperature 0.4 K higher than attained without the neon overcoat, resulted in a 30% reduction in DA and almost complete removal of the 1918.3, 1845.1, 1362.8, 1306.6, and 1227.8, 752.8 cm^{-1} band set (labeled R) (Table 2), while the bands at 1942.0, 1919.9, 1816.7, 851.5, and 726.7 cm^{-1} (labeled TA) (Table 3) remained unchanged, and the 1925, 1914, 1871, and 770 cm^{-1} bands (group 4) (Table 4) increased markedly. Note also a reversal in the intensities of site split DA bands (Figure 1e). In another experiment, a subsequent $\lambda > 240$ nm irradiation restored the original DA site band intensities. Next, annealing to 8 K decreased the AlH_3 absorptions, reduced the seven DA bands by 80% in concert, increased the 1925, 1914,

TABLE 3: Comparison of Calculated and Observed Frequencies (cm^{-1}) for Trialane Al_3H_9

SCF/DZP[a,b]	B3LYP/6-311++G(d,p)[c]	observed
2094 (285) e′	1991 (195 × 2) e	1942[d]
2066 (648) a_2''	1985 (564) a_1	1920
2061 (0) a_1'	1966 (13) a_1	
2060 (0) e″	1978 (10 × 2) e	
1980 (1578) e′	1910 (1265 × 2) e	1817
1853 (0) a_2'	1839 (0) a_2	
1128 (0) a_1'	1047 (0) a_1	
962 (570) a_2''	805 (319) a_1	
952 (800) e′	912 (414 × 2) e	851
872 (0) e″	759 (0 × 2) e	
813 (0) a_1'	747 (0) a_1	
771 (806) e′	710 (577 × 2) e	726
614 (156) e′	583 (191 × 2) e	

[a] Ref 3. Intensities, km/mol, in parentheses. D_{3h} structure: Al−H−Al: 1.702 Å and 140.2°, Al−H_2: 1.566 Å and 128.3°. Strong bridge mode is 1980 cm^{-1}. [b] Seven frequencies 544−72 cm^{-1} (0 to 10 km/mol) are omitted. [c] This work: C_{3v} structure: Al−H−Al, 1.702 Å, 142.3°, Al−H_2: 1.576 Å, 128.3°. [d] Al_3D_9 counterpart 1401 cm^{-1}.

TABLE 4: Comparison of Calculated and Observed Frequencies (cm^{-1}) for Tetraalane Al_4H_{12}

SCF/DZP[a]	B3LYP/6-311++G(d,p)[b]	observed[c]
2183 (342 a_1	2050.3 (0)	
2066 (715) a_1	1991.1 (682)	1925
2062 (0) a_1	1981.1 (0)	
2058 (0) a_1	1973.3 (0)	
2020 (215) a_1	1942.4 (0)	
982 (0) a_1	830.1 (11)	
956 (633) a_1	874.4 (429)	770
810 (0) a_1	821.3 (0)	
767 (332) a_1	774.2 (12)	
2130 (1290 b_2 and b_2	2020.1 (1034)	
2060 (133) b_1 and b_2	1984.9 (43)	1914
2014 (1334) b_1 and b_2	1942.8 (1384)	1871
895 (117) b_1 and b_2	731.0 (25)	
777 (1267) b_1 and b_2	702.8 (1744)	masked
618 (141) b_1 and b_2	729.7 (8)	

[a] Ref 4. Intensities, km/mol, in parentheses, C_{2v} symmetry: terminal Al−H_2 1.566 Å, 127.1°; bridged Al−H−Al 1.694 Å, 170.7°. [b] This work. C_{2v} symmetry: terminal Al−H_2 1.575 Å, 127.9°; bridged Al−H−Al 1.699 Å, 156.5°. [c] Group 4 bands.

1871, and 770 cm^{-1} bands (group 4) while the 1942.0, 1919.9, 1816.7, 851.5, and 726.7 cm^{-1} bands (TA) remained constant. Further temperature increase allowed the H_2 matrix to evaporate and produced the broad 1720 and 720 ± 20 cm^{-1} bands assigned previously to solid alane.[1,2]

Another experiment employed 193 nm laser irradiation and generated different relative product yields; Figure 2 illustrates the resulting spectra and shows AlH_3, Al_2H_4, AlH_2, AlH_4^-, AlH, and Al_2H_2 absorptions as reported previously.[1,2,7,12−15,19] Irradiation at $\lambda > 380$, 320, and 290 nm increased AlH_3 at the expense of AlH and increased AlH_4^- at the expense of a 3972 cm^{-1} absorption that we believe is due to $(H^-)(H_2)_n$.[20] In addition, weak DA bands appear and Al_2H_2 is destroyed.[12,20] Irradiation at $\lambda > 240$ nm, Figure 2b, markedly increases the DA bands, decreases AlH_4^-, and forms the R band set. Next, irradiation at 193 nm increased the DA and R bands by about 2.5 times and increased AlH_2 at the expense of Al_2H_4, but continued 193 nm irradiation further increased DA and not R absorptions, Figure 2c−e. Very weak TA bands were observed, but no evidence was found for group 4 absorptions. Satellite absorptions were revealed at 1824.8 and 1790.2 cm^{-1} on AlH_2 bands at 1822.1 and 1788.0 cm^{-1}; such bands have been characterized as $(H_2)AlH_2$ complexes.[7] Subsequent annealing

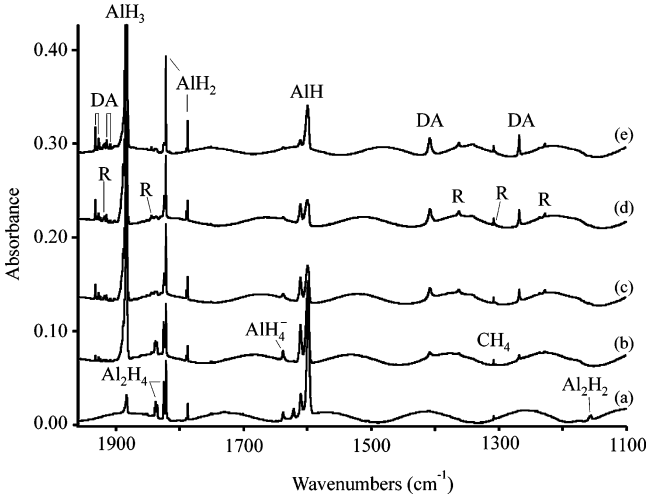

Figure 2. Infrared spectra in the 1960−1100 cm^{-1} region for laser-ablated Al using 30 mJ/pulse co-deposited with normal hydrogen at 3.5 K. (a) Spectrum of deposited sample, (b) after $\lambda > 240$ nm irradiation at 5.4 K for 20 min, (c) after 193 nm irradiation for 10 min using 17 mW, (d) after 10 min more 193 nm irrradiation, and (e) after 10 min more 193 nm irrradiation.

to 6.5 K decreased the bands as before, and removing the H_2 matrix again formed the strong, broad 1720 and 720 cm^{-1} absorptions.

Manceron has prepared AlH_3 by exciting the $A^1\Pi \leftarrow X\ ^1\Sigma^+$ transition of AlH in the region 365−404 nm; the gas-phase band origin is 23 470 cm^{-1}.[14,16,21] We find that the production of AlH_3 in solid hydrogen is more efficient with the full mercury arc, which should also reach the $C\ ^1\Sigma^+$ state with gas-phase origin at 44 676 cm^{-1}.

The H−H, H−D, and D−D fundamental regions are compared in Figure 3 for solid H_2, HD, and D_2 samples. Several new absorptions are noteworthy: The induced $H_2[D_2]$ fundamentals[22] are observed at 4152.8 [2986.8] cm^{-1} followed by sharp 4143.4 [2982.4] cm^{-1} absorptions that decrease on sample irradiation. Next are broad 4108.7 [2959.4] cm^{-1} bands that decrease on photolysis into sharp features. Such absorptions were not observed in p-H_2 experiments with thermal Al atoms following irradiation.[2] Sharp 4061.6 [2919.6] cm^{-1} absorptions appear on UV irradiation and track with the strong 1883.7 [1378.7] cm^{-1} $AlH_3[AlD_3]$ bands so it is straightforward to associate these absorptions. A 4069.5 cm^{-1} counterpart for the 1885.3 cm^{-1} AlH_3 band was observed in p-H_2.[2] Finally, broader photosensitive 3972 [2870] cm^{-1} absorptions have been assigned to $(H^-)(H_2)_n[(D^-)(D_2)_n]$ complexes.[20] The HD counterparts of these bands are observed at 3624.7, 3621.7, 3591.7, 3548.7, and 3478 cm^{-1}, respectively.

Corresponding experiments were done with pure D_2. The freshly deposited spectrum reveals AlD_3, Al_2D_4, AlD_2, AlD_4^-, AlD, and the new AlD_2^- species[2] (Figure 4a). Irradiation with filtered mercury arc light ($\lambda > 380$, 320, and 290 nm) decreased AlD_2^- and $(D^-)(D_2)_n$ at 2870 cm^{-1} and increased AlD_4^-. Spectra following the 380 and 290 nm irradiation are shown in Figure 4b,c. Full arc irradiation decreased AlD_4^-, destroyed AlD_2^-, and produced weak DA absorptions at 1415.0, 1028.5, 607.5, and 510.6 cm^{-1} (Figure 4d). Next, 193 nm irradiation for 10 min doubled AlD_3, increased DA absorptions 5-fold, reduced AlD, AlD_2, and Al_2D_4, destroyed AlD_4^-, and reproduced 20% of the $(D^-)(D_2)_n$ signal at 2870 cm^{-1}. In addition, the weaker 919.9 cm^{-1} DA absorption and a new 459.1 cm^{-1} DA absorption were observed, and very weak 1403.2, 1353.6, 991.8 cm^{-1} bands appear and track together (Figure 4e). The latter bands increase markedly on annealing to 7.8 K, and a weaker 899.2 cm^{-1} absorption joins them while the DA bands increase slightly and a weak AlD_4^- band reappears (Figure 4f). The Al−D−Al bridge stretching modes are split bands at 1036.2, 1031.6, 1028.5 and 931.6, 925.2, 919.9 cm^{-1}; subsequent alternating annealing and 193 nm irradiation cycles swap site absorption intensities (not shown). Likewise, 193 nm radiation destroys the 1403.2, 1353.6, and 991.8 cm^{-1} band pair, and further annealing increases them with the same relative intensity.

Two additional experiments were done with Al and pure HD, and spectra are illustrated in Figure 5. The product yield is higher than reported previously, and the numerous isotopic product absorptions are more clearly observed. The spectrum

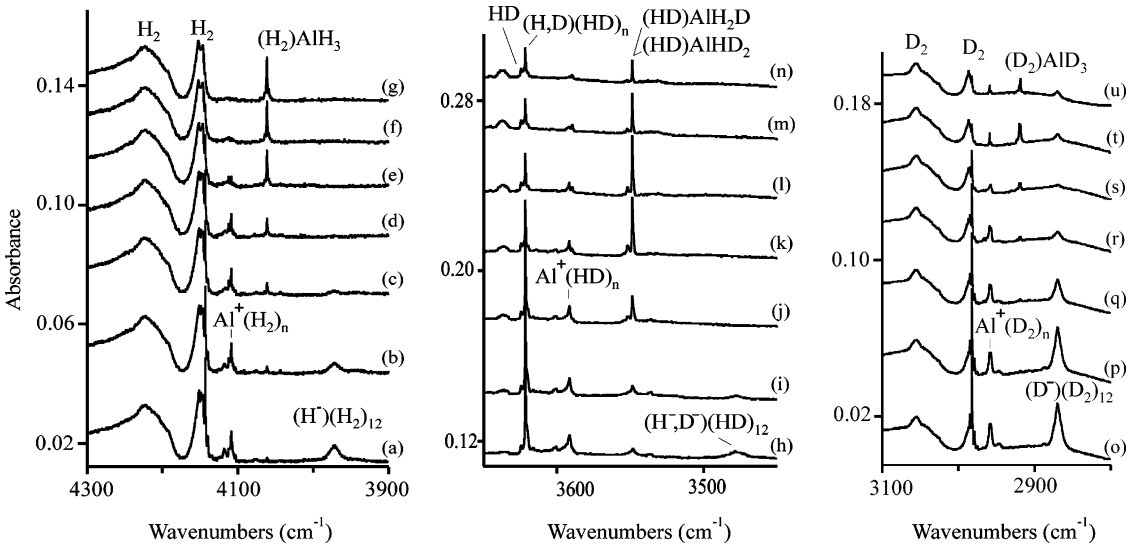

Figure 3. Infrared spectra in the 4300−3900, 3650−3450, and 3100−2800 cm^{-1} regions for laser-ablated Al using 30 mJ/pulse co-deposited with hydrogen, HD, and deuterium, respectively, at 3.5 K. (a) Spectrum of deposited Al + H_2 sample, (b), (c), (d), (e) after $\lambda > 380$, 320, 290, and 240 nm irradiations, respectively, (f) after 193 nm irradiation, (g) after additional 193 nm irradiation, (h) spectrum of deposited Al + HD sample, (i), (j), (k), after $\lambda > 380$, 290, and 240 nm irradiations, respectively, (l), (m), (n) after annealing to 6.0, 7.0, and 8.2 K, (o) spectrum of deposited Al + D_2 sample, (p), (q), (r), (s) after $\lambda > 380$, 320, 290, and 240 nm irradiations, respectively, (t) after 193 nm irradiation, and (u) after annealing to 7.8 K.

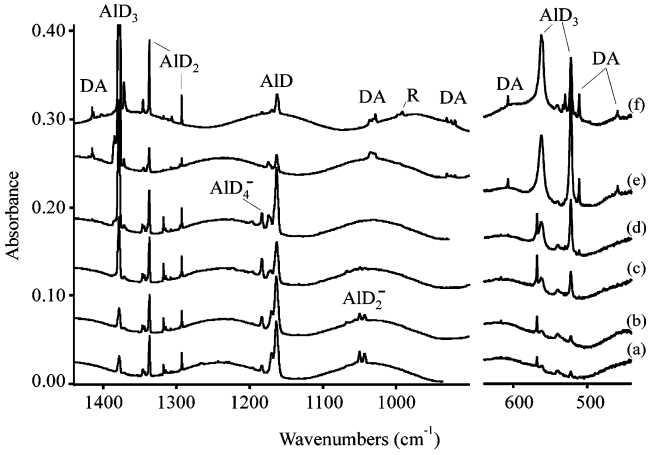

Figure 4. Infrared spectra in the 1440−900 and 640−440 cm^{-1} regions for laser-ablated Al using 30 mJ/pulse co-deposited with normal deuterium at 3.5 K. (a) Spectrum of deposited Al + D_2 sample, (b), (c), (d), (e) after λ > 380, 320, 290, and 240 nm irradiations, respectively, and (f) after annealing to 7.8 K.

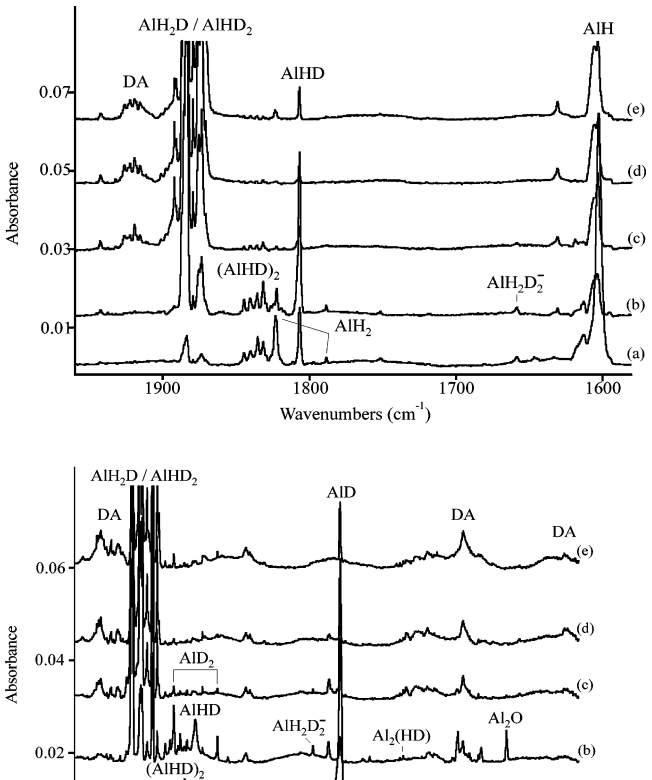

Figure 5. Infrared spectra in the 1960−1580 cm^{-1} region (part A) and 1440−970 cm^{-1} region (part B) for laser-ablated Al using 40 mJ/pulse co-deposited with pure HD at 3.5 K. (a) Spectrum of the deposited sample, (b) after λ > 290 nm irradiation, (c) after λ > 240 nm irradiation at 3.5 K, (d) after λ > 240 nm irradiation at 6.0 K, and (e) after λ > 240 nm irradiation at 7.0 K.

from the deposited sample is dominated by AlH and AlD absorptions at 1602.5 and 1166.4 cm^{-1}, which are blue-shifted 3.8 and 3.3 cm^{-1} from their H_2 and D_2 matrix counterparts, respectively.[1,2] The AlHD species is observed at 1806.7 and 1315.4 cm^{-1}, and weaker bands are observed for AlH_2 and AlD_2. The new bands at 1844.6, 1840.3, 1835.2, and 1831.6 cm^{-1} in the Al−H region and at 1346.3, 1341.5, 1330.8, and 1326.7

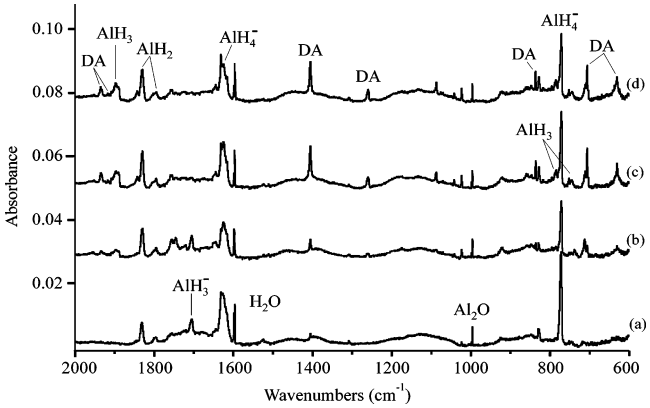

Figure 6. Infrared spectra in the 2000−600 cm^{-1} region for laser-ablated Al using 30 mJ/pulse co-deposited with 1% H_2 in neon at 3.5 K. (a) Spectrum of deposited sample, (b) after 193 nm irradiation for 13 min using 40 mW, (c) after λ > 240 nm irradiation for 10 min, and (d) after annealing to 7.5 K.

cm^{-1} are due to four stretching modes (and site splittings) for AlHDAlHD.

The bands of most interest here occur in the 1920, 1410, and 1030 cm^{-1} regions. First, sharp bands at 1932.5, 1926.5, 1922.6, 1919.4, and 1915.8 cm^{-1} are in the region of the terminal Al−H_2 stretching modes of Al_2H_6.[1,2] The 1932.5 cm^{-1} band is probably due to Al_2H_6, and the other bands are due to X_2Al-(μ-X)$_2$Al−H_2 stretching modes (X = H or D). Our isotopic frequency calculations show relatively little coupling between the dialane vibrational modes, and accordingly changing X has little effect on the terminal Al−H_2 modes. Likewise in the 1410 cm^{-1} region, the sharp 1416.7, 1415.0, 1412.9, and 1402.2 cm^{-1} bands are due to terminal Al−D_2 stretching modes. However, the broader 1414 and 1395 cm^{-1} features are appropriate for $X_2Al(\mu\text{-}H)_2AlX_2$ bridge stretching modes shifted in both directions from the 1408 cm^{-1} value for Al_2H_6, based on our calculations. Finally, the two bands at 1039.7 and 935.0 cm^{-1} go together and are just above 1036.2 and 931.6 cm^{-1} major site bands for the Al−D−Al bridge stretching modes of Al_2D_6. The 1039.7 and 935.0 cm^{-1} bands are clearly due to such bridge modes for $X_2Al(\mu\text{-}D)_2AlX_2$ molecules. Although no assignments can be made to particular mixed H, D dialane molecules, shifted bands were observed in pure HD that follow our earlier assignments to Al_2H_6.

After annealing to remove the HD matrix host, two broad bands remain centered at 1790 and 1310 cm^{-1}. These are higher than the broad $(AlH_3)_n$ and $(AlD_3)_n$ bands at 1720 and 1260 cm^{-1}.[1,2] The shift to higher frequency for the solid alane mixed H, D compound points to different coupling of the Al−H−Al and Al−D−Al modes and suggests that a symmetric Al−H−Al mode will be found at higher frequency in the Raman spectrum of solid alane.

Several more neon matrix experiments were done with dilute H_2, and better spectra were obtained for dialane and aluminum hydride anion species. Figure 6 illustrates spectra from an experiment with 1% H_2 and the same ablation laser energy employed for the pure hydrogen experiments. Irradiation at 193 nm increases the AlH and AlH_2 bands at 1610.8, 1828.6, and 1794.7 cm^{-1}, but λ > 240 nm irradiation increases these bands even more and produces a weak AlH_3 band at 1889 cm^{-1} and the seven dialane bands listed in Table 5. The DA bands are sharper and stronger than observed in our first investigation.[2] Note that annealing to 7.5 K *does not* increase the DA bands. An additional λ > 240 nm irradiation did not increase the DA intensities, and a subsequent 10 K annealing decreased the DA

TABLE 5: Comparison of Aluminum Hydride and Dialane Frequencies (cm^{-1}) Observed in Solid Neon, p-H_2, and n-H_2 at 2−4 K

neon	p-H_2[a]	n-H_2	molecule, mode
	3155.3	3141.4	AlH, complex 2ν
	1618.4	1610.7	AlH, R (0)
1610.8	1606.1	1598.7	AlH, complex ν
1828.6	1825.0	1821.9	AlH_2, ν_3 (b_2)
1794.7	1790.2	1787.8	AlH_2, ν_1, (a_1)
1889.1	1885.5	1883.7	AlH_3, ν_3 (e)
1935.0	1933.5	1932.3	Al_2H_6, b_{1u}
1916.6	1916.0	1915.1	Al_2H_6, b_{3u}
1404.7	1406.1	1408.1	Al_2H_6, b_{3u}
1259.4	1264.3	1268.2	Al_2H_6, b_{2u}
835.6	835.2	835.6	Al_2H_6, b_{1u}
705.3		702.4	Al_2H_6, b_{3u}
629.6		631.9	Al_2H_6, b_{2u}

[a] Ref 2 from photolysis of Al in p-H_2. BaF_2 substrate limits reliability of spectra below 800 cm^{-1}. The R(0) overtone is observed at 3180.3 cm^{-1}.

intensity slightly (not shown). Similar results were obtained for 0.1% and 0.4% H_2 samples. Irradiation at $\lambda > 530$ nm destroyed the 1706.0 cm^{-1} band, and $\lambda > 240$ nm had the same noteworthy effect of producing DA as shown in Figure 6c, but a subsequent 193 nm irradiation restored the 1706.0 cm^{-1} band and decreased AlH_3 and Al_2H_6 bands. In summary, Al_2H_6 increases on annealing in pure hydrogen experiments, but irradiation that fosters the growth of AlH_3 increases the yield even more. This suggests that the exothermic[2,8,18] dimerization reaction has a small activation energy.

The deposited neon samples also revealed strong 1626 and 770.2 cm^{-1} and weak 1523.0 cm^{-1} bands that are due to AlH_4^-; no absorptions were observed in the 1400−1450 cm^{-1} region. Finally, warming the neon samples above 14 K to remove the neon host gave a very weak, broad 1720 cm^{-1} absorption in the same position as found in our hydrogen experiments.

After this aluminum hydride report was completed, we developed a simple method for making high (99%) purity p-H_2 and o-D_2 using $Fe(OH)_3$ catalyst in a copper tube immersed in the cold gas over liquid helium. Laser-ablated Al experiments gave p-H_2 and o-D_2 counterparts for the major absorptions, which are compared in a new Table Added in Proof. The important comparison to notice is that the dialane terminal Al-H [Al-D] stretching frequencies are about 1 cm^{-1} higher in the less interacting $J = 0$ solids than in the normal solids, and the bridge Al-H stretching modes are 1−3 cm^{-1} lower in the $J = 0$ solids. Clearly the dialane bridge bonds are more vulnerable to intermolecular interactions.

Al_2H_5 Radical. Calculations were done for Al_2H_5 radicals in C_s and C_{2v} structures corresponding to dialane minus one hydrogen from the terminal or bridged positions (Figure 7). The dibridged structure is 6.0 kcal/mol lower in energy, and the bond lengths and angles are very much the same as calculated for Al_2H_6 at the same B3LYP level of theory. The terminal AlH_2 and dibridged Al−H frequencies are slightly lower than dialane values, and the single Al−H frequency is lower (Table 6). The monobridged radical has two terminal AlH_2 groups almost identical to dialane and 6−19 cm^{-1} lower frequencies.

Computations were also done for Al_2H_3 radicals. The $^2A''$ structures $HAlAlH_2$ and $HAl(\mu\text{-}H)_2Al$ had significant imaginary frequencies. Two $^2A'$ structures of the mono and dibridged form have essentially the same energy; their frequencies are listed in Table 6.

The band set labeled R is assigned to the dibridged Al_2H_5 radical (Figure 2) on the basis of new bands in the terminal Al−H_2 and bridged Al−H−Al stretching regions. Calculated

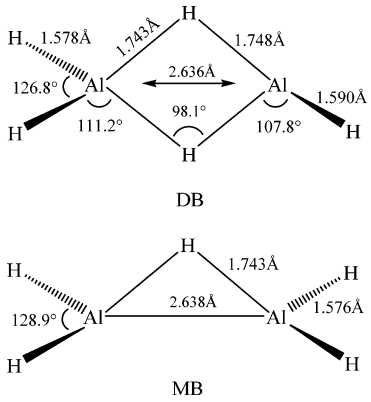

Figure 7. Structures calculated (B3LYP/6-311++G**) for dibridged (DB) and monobridged (MD) Al_2H_5 radicals.

frequencies are higher than observed (Table 2) by amounts (33−59 cm^{-1}) comparable to that found for Al_2H_6 itself.[1,2] Note on annealing (Figure 1) Al_2H_5 bands appear and decrease before Al_2H_6 bands do on successive annealing cycles. This is consistent with behavior expected for a species made from smaller fragments (AlH_2, AlH_3) and a free radical. The monobridged Al_2H_5 radical isomer that is 6.0 kcal/mol higher in energy (Table 6) was not trapped. In the Ga/H_2 system both Ga_2H_5 radical isomers were observed, but their calculated energy separation was only 1 kcal/mol.[23]

(H_2)AlH_3 Complex. The sharp bands at 4061.6 [2919.6] cm^{-1} that increase on irradiation in parallel with the 1883.7 [1378.7] cm^{-1} AlH_3 [AlD_3] bands are assigned to the H−H[D−D] stretching modes in a weak 3-center-2-electron bonded complex (Figure 3). The H/D ratio 1.3911 is appropriate for this vibration. In pure HD the counterpart absorbs at 3548.7 cm^{-1}. This means that AlH_3 exists as the (H_2)AlH_3 complex in solid H_2. In p-H_2, the (H_2)AlH_3 complex is observed at 4069.5 and 1885.5 cm^{-1}.[2] We find a 4064.4 cm^{-1} satellite on the 4061.6 cm^{-1} n-H_2 band and a 4063.8 cm^{-1} satellite on the 4069.3 cm^{-1} band in enriched p-H_2: The satellites are probably due to the minor nuclear spin isomer in the complex which is dominated by the major nuclear spin isomer of the solid host.

Calculations at the MP2 level (Table 7) support this bonding picture and reveal a 0.1 kcal/mol binding energy. The ν_3 (e) mode of isolated AlH_3 is split 3 cm^{-1} in the (H_2)AlH_3 complex, which is within the experimental 1883.7 cm^{-1} bandwidth. Our calculation also predicts a H−H fundamental in the complex red-shifted 135 cm^{-1} from the H_2 value. Computational attempts to bind a second H_2 ligand led to its dissociation. The H−H stretching mode in the (H_2)AlH_3 complex is red-shifted 91 cm^{-1} from the H−H fundamental in solid hydrogen. This is enough to characterize a significant weak H_2−AlH_3 interaction in this "hypervalent" complex. In contrast, (H_2)GaH_3 supported a smaller 66 cm^{-1} shift for the dihydrogen ligand.[23]

Al_3H_9 Trialane. The group 3 product absorptions appeared after Al_2H_6 and remained on final annealing. These bands follow calculated frequencies for trialane. The structure of trialane and the most notable property, discussed previously by Duke et al.,[3] is that the Al−H−Al bridge bond has a larger angle (140°) than dialane (98°) and the bridge stretching frequency is substantially higher than found for dialane, whereas the terminal Al−H_2 units are similar in structure and frequency for these two molecules. Accordingly the five frequencies (Table 3) are assigned to Al_3H_9.

Al_4H_{12} Tetraalane. Calculations from the Schaefer group[4] found that tetraalane is most stable in a C_{2v} "butterfly" structure with slightly shorter (1.694 Å) and more nearly linear (170.7°) Al−H−Al bridge bands than computed for trialane. Accord-

TABLE 6: Calculated (B3LYP/6-311++G(d,p)) Structures and Frequencies for Aluminum Hydride Species

molecule	lengths, Å, angles	frequencies, cm^{-1} (intensities, km/mol)
Al_2H_3 ($^2A'$)[a] (MB)	1.584, 1.694, 1.957, 2.669 127.6[a], 93.7[b], 115.3	1944 (216), 1921 (120), 1448 (152), 937 (662), 724 (81), 698 (377), 433 (13), 245 (1), 174 (16)
Al_2H_3 ($^2A'$)[a] (DB)	1.584, 1.679, 1.920, 122.2, 94.2[b]	1917 (317), 1624 (75), 1495 (50), 1014 (513), 964 (242), 658 (81), 437 (1), 371 (36), 74 (6)
Al_2H_5 ($^2A'$)[c] (DB)	1.578, 1.590, 1.743, 1.748, 111.2[b], 98.1	1970 (a′, 210), 1951 (a′, 99), 1887 (a′, 166), 1535 (a′, 13), 1422 (a′, 1017), 1345 (a″, 108), 1261 (a″, 173), 806 (a′, 213), 736 (a′, 339) 704 (a″, 25), 553 (a″, 101), 519 (a′, 56) 433 (a″, 2), 266 (a′, 1), 237 (a′, 12)
Al_2H_5 ($^2A_1$)[c] (MB)	1.576, 1.743 128.9[b], 98.4	1983 (b_1, 408), 1975 (a_2, 0), 1957 (a_1, 3), 1947 (b_2, 171), 1421 (b_2, 557), 1264 (a_1, 196) 778 (b_1, 132), 727 (a_1, 2), 689 (b_2, 551), 577 (a_1, 205), 455 (a_2, 0), 398 (b_2, 21) 296 (a_1, 1), 286 (a_2, 0), 217 (b_1, 12)
Al_2H_6 (^1A_g) (DA)	1.575, 1.740, 128.0[b], 97.6	1989 (b_{1u}, 419), 1981 (b_{2g}, 0), 1972 (a_g, 0) 1966 (b_{3u}, 126), 1546 (a_g, 0), 1483 (b_{3u}, 1096) 1402 (b_{1g}, 0), 1292 (b_{2u}, 353), 866 (b_{1u}, 244), 766 (b_{3g}, 0), 754 (a_g, 0), 712 (b_{3u}, 648), 634 (b_{2u}, 263), 484 (b_{2g}, 0), 475 (b_{2g}, 0), 423 (a_u, 0), 374 (a_g, 0), 223 (b_{1u}, 13)
AlH^- ($^2\Pi$)[d]	1.703	1472 (1259)

[a] The monobridged isomer is 0.6 kcal/mol lower in energy at the B3LYP level. [b] Terminal AlH_2 angle. [c] Bridge Al−H−Al angle. The dibridged (DB, $^2A'$) isomer of Al_2H_5 is 6.0 kcal/mol lower in energy than the (MB, $^2A_1$) isomer. [d] AlH^- is 5.0 kcal/mol lower in energy than AlH.

TABLE 7: Calculated (MP2/6-311++G(3df, 3pd) Structures and Frequencies for Aluminum and Gallium Hydride Species

molecule	lengths, Å	frequencies, cm^{-1} (intensities, km/mol)
H_2 ($^1\Sigma_g^+$)	0.737	4515 (0)
$Al^+(H_2)$ ($^1A_1$)	3.078, 0.741	4454 (61) a_1, 358 (5) b_2, 174 (25) a_1
$Ga^+(H_2)$ ($^1A_1$)	3.020, 0.741	4455 (61) a_1, 357 (6) b_2, 188 (15) a_1
AlH- -HH ($^1\Sigma$)	1.646, 2.694, 0.738	4497 (11), 1723.7 (776), 245 (0 × 2), 90 (0), 28i (0 × 2)
AlH ($^1\Sigma^+$)[a]	1.645	1724.2 (717)
AlH_3 ($^1A_1'$) (D_{3h})	1.575	1995.2 (0), 1994.7 (276 × 2), 820.6 (238 × 2), 730.9 (387)
$(H_2)AlH_3$ (C_s)	2.256, 0.746, 1.576	4380 (21), 1989 (47), 1985 (251), 1982 (256), 817 (168), 809 (223), 774 (54), 741 (444), 402 (1), 390 (1), 312 (47), 31i (0)
$(H_2)GaH_3$ (C_s)	2.477, 0.743, 1.577	4424 (17), 2013 (4), 1998 (286), 1995 (282), 777 (174), 777 (170), 728 (278), 604 (5), 317 (0), 312 (0), 233 (23), 15i (0)

[a] Dipole moment 0.11 D (0.23 D using B3LYP).

ingly, the appearance of a strong 1871 cm^{-1} absorption on late annealing above the bridge mode of trialane (1817 cm^{-1}) suggested the higher alane. The accompanying absorptions at 1925, 1914, and 770 cm^{-1} are also appropriate for tetraalane. Note that the terminal Al−H_2 groups are little affected and these frequencies change little in the dialane, trialane, and tetraalane series. Again, warming to evaporate the H_2 matrix allowed further reaction to form the solid alane film characterized by broad 1720 and 720 cm^{-1} absorptions.[1,2]

$Al^+(H_2)_n$. The sharp, photosensitive 4108.7 cm^{-1} absorption in solid hydrogen with 2959.4 cm^{-1} solid deuterium counterpart is shifted just 44 cm^{-1} from the solid hydrogen fundamental (Figure 3). The H/D ratio, 1.3884, is just below the 4152.8/2986.8 = 1.3904 value for the solid fundamental.[22] The addition of 0.03% CCl_4 to these samples to serve as an electron trap eliminated the following negative ion bands and enhanced the 4108.7 [2959.4] cm^{-1} absorptions 5-fold, which is appropriate behavior for a cation absorption. The HD matrix revealed an intermediate band at 3591.7. Calculations show that the most stable structure is the side bound $Al^+(H_2)$ complex rather than $(H-Al-H)^+$,[24,25] and this energy difference is 13 kcal/mol at the CCSD(T) level. Our MP2 computation predicts the H−H frequency in the $Al^+(H_2)$ complex to be red-shifted 61 cm^{-1}. Our solid hydrogen observation shows a smaller red shift (44 cm^{-1}) because many H_2 ligands are interacting with Al^+ in the solid H_2 lattice as the $Al^+(H_2)_n$ complex. In a substitutional site, Al^+ can complex with 12 H_2 ligands. The laser-ablation plume contains a substantial proportion of Al^+ cations, and it is reasonable to expect some of these Al^+ cations to be trapped in the solid hydrogen matrix as an $Al^+(H_2)_n$ complex. The Ga^+ counterparts are observed 4108.9 and 2960.4 cm^{-1} in the solid molecular hydrogens.[23]

To gain more understanding of the laser-ablation process, emission from the laser-ablation plume was examined using an optical fiber spectrometer. The spectrum illustrated in Figure 8 reveals strong gas-phase Al($^2S \rightarrow {}^2P$ and $^2D \rightarrow {}^2P$) emissions at 396.3 and 308.3 nm, respectively, strong Al^+ lines at 358.6 and 624.3 nm, and weaker Al lines at 256.9, 265.3, and 708.5 nm and Al^+ at 281.6 nm from the region between the metal target and cold window.[26,27] The relative intensity of Al and Al^+ emissions is determined by ablation laser energy focused on the target; reducing the laser energy reduces both but the Al^+ emission decreases in greater proportion with lower power density. Since the Al and Al^+ transition probabilities are comparable,[27] emission spectra reveal approximately the relative number of ablated Al and Al^+ species, which relax and perform matrix chemistry.[25] The role of Al^+ in laser-ablated aluminum trapped in p-H_2 has been discussed.[28] Clearly Al^+ cations are

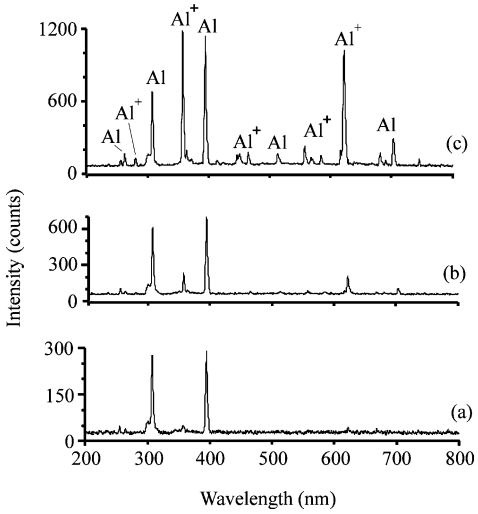

Figure 8. Emission spectra from 1064 nm laser-ablated aluminum plume between target and cold window (10 ns pulse, 10 cm f.l.). (a) Laser energy 20 mJ/pulse, (b) laser energy 30 mJ/pulse, and (c) laser energy 40 mJ/pulse.

present in the ablated material,[29] and their chemistry (which includes electron recombination to form excited Al*) must be considered.

Excimer laser (193 nm)-induced fluorescence was next examined from the cold samples. Both solid H_2 and solid D_2 gave only background emissions. Under 193 nm excitation, the reaction of Al in solid molecular hydrogen is complete. However, in solid neon a strong, sharp 301.1 nm $^2D \rightarrow {}^2P$ atomic emission is observed without the $^2S \rightarrow {}^2P$ emission counterpart. A broader 351 nm band increases on annealing and a very broad 610 nm emission appears—the latter are probably due to Al_x cluster species. The sharp $^2D \rightarrow {}^2P$ Al emission is blue-shifted 770 cm^{-1} from the gas-phase value. Previous Al emissions in solid matrices are Stokes-shifted from the corresponding matrix absorptions owing to differences in relaxation dynamics.[30,31]

Molecular Anions. Our observation of AlD_2^- at 1050.0 and 1043.0 cm^{-1} in solid D_2 is interesting in part because AlH_2^- is too reactive to survive condensation in solid hydrogen.[2] Figure 4 shows the decrease in AlD_2^- absorptions with increase in AlD_4^- at 1183.2 cm^{-1} with successive irradiations at $\lambda > 380$, 320, and 290 nm; $\lambda > 240$ nm completely destroyed AlD_2^- and even decreased AlD_4^-. Neon matrix samples revealed AlD_2^- slightly blue-shifted at 1056.9 and 1049.3 cm^{-1}. Additional neon matrix experiments were performed to look for AlH_2^-, but no absorption was observed in the expected 1400−1450 cm^{-1} region although the 1626 cm^{-1} AlH_4^- band was strong. We note that the isoelectronic SiH_2 molecule was not observed in solid hydrogen, but SiH_2 was isolated in solid neon under analogous conditions.[10,32]

The dynamics in the condensation processes for H_2 and D_2 at our 3.5 K substrate temperature are slightly different. Hydrogen (FP = 13.9 K) freezes more slowly than deuterium (FP = 18.7 K).[33] Hence, AlH_2^- formed during the condensation process will be quenched less effectively than AlD_2^-, and the reaction of AlH_2^- in condensing H_2 is spontaneous whereas some AlD_2^- survives in solid deuterium.

$$AlH_2^- + H_2 \rightarrow AlH_4^- \quad [\Delta E = -45 \text{ kcal/mol}]^2 \qquad (1)$$

$$AlD_2^- + D_2 \rightarrow AlD_2^-(D_2) \text{ and } AlD_4^- \qquad (2)$$

A sharp weak photosensitive 1701.6 cm^{-1} absorption was considered for AlH_3^- in our earlier paper.[2] A sharp weak 1246.9 cm^{-1} counterpart in solid D_2 is also destroyed by $\lambda > 380$ nm irradiation and exhibits a 1.365 H/D ratio. Several solid neon experiments reveal a higher yield of this feature at 1706.0 cm^{-1} and give the deuterium counterpart at 1250.8 (H/D ratio 1.364). These observations support assignment to AlH_3^-. Recall that a strong ν_3 (e) mode was predicted at 1698 cm^{-1} by B3LYP calculations.[2] We find that AlH_3^- photodetaches with $\lambda > 530$ nm radiation, which is above the 10 kcal/mol electron affinity estimate from B3LYP calculations.[2] It is interesting that subsequent 193 nm irradiation increases AlH_3^- at the expense of AlH_3 in solid neon. This arises from photoionization of Al in the matrix with subsequent electron capture. We observed $(D^-)(D_2)_n$ growth with 193 nm irradiation of Al in solid deuterium.[20]

$$AlH_3^- \xrightarrow{\lambda > 530 \text{ nm}} AlH_3 + e^- \qquad (3)$$

The ultimate anion in these experiments is the hydride anion trapped in the solid H_2 lattice, which gives the super complex $(H^-)(H_2)_{12}$. The photosensitive 3972 cm^{-1} absorption arises from this complex as has been discussed in a recent publication.[20]

Conclusions

The new aluminum hydride species characterized here exhibit interesting chemistry.

AlH_3 Association Reaction. We found in these hydrogen and neon matrix reactions that annealing alone (5−8 K in solid hydrogen and 5−12 K in solid neon) does not significantly increase the yield of dialane, but UV irradiation, particularly $\lambda > 240$ nm, increases AlH_3 and Al_2H_6 markedly. Even irradiation with a Nernst glower appeared to assist the formation of dialane. Since the trigonal planar AlH_3 molecule must deform out-of-plane slightly to fit into the dibridged Al_2H_6 structure, a small activation energy is apparent for reaction 4. However, in solid neon the AlH_3 yield is so small that another mechanism must operate. At low H_2 concentration, Al can dimerize and then react with H_2. Both Al_2H_2 and Al_2H_4 are observed on deposition of thermal Al atoms into p-H_2, but photolysis was required to form AlH_3 and Al_2H_6.[2] In our solid neon experiments Al_2 apparently reacts on photolysis straight-away with clustering H_2 molecules to form Al_2H_6 as no Al_2H_2 nor Al_2H_4 were trapped. It appears that the formation of trialane requires activation but that the addition of AlH_3 to Al_3H_9 is spontaneous as is the formation of solid alane on removal of the hydrogen or neon matrix, reaction 8.

$$AlH_3 + AlH_3 \xrightarrow{E_a} Al_2H_6 \quad [\Delta E = -34 \text{ kcal/mol}]^2 \qquad (4)$$

$$Al_2 + 3H_2 \xrightarrow{h\nu} Al_2H_6 \quad [\Delta E = -87 \text{ kcal/mol}]^2 \qquad (5)$$

$$AlH_3 + Al_2H_6 \xrightarrow{E_a} Al_3H_9 \qquad (6)$$

$$AlH_3 + Al_3H_9 \rightarrow Al_4H_{12} \qquad (7)$$

$$nAlH_3 \rightarrow \frac{1}{n}(AlH_3)_n \qquad (8)$$

We pointed out in our first dialane paper[2] that 6.5 K annealing increases AlH_2 from the AlH + H combination reaction, and the small growth of Al_2H_4 and Al_2H_6 on annealing must also come from H atom reactions. Knight finds very strong ESR signals for H atoms trapped in solid hydrogen following laser-ablation co-deposition,[34] and H atom reactions are responsible for much of the chemistry observed on annealing. Finally, the sharp lines at 4143.4 [2982.4] cm^{-1} in solid hydrogen [deute-

rium] (Figure 3) decrease on annealing in other samples and are common to all of our laser-ablated metal atom experiments. These sharp bands are probably due to H [D] atoms trapped in the solids, which perturb and slightly shift the solid H_2 [D_2] vibrational mode.

Alane oligomers have been formed on Al(111) surfaces, and these oligomers are characterized by a broad 1500−1800 cm^{-1} band centered at 1660 cm^{-1} for Al−H−Al bridge and sharper 1880 cm^{-1} band for terminal Al−H stretching frequencies.[35] We note that the surface 1880 cm^{-1} band is just below all of the higher alane molecule terminal modes observed here (1942−1914 cm^{-1}), which is reasonable for a surface absorption, and that the broad 1500−1800 band almost matches our broad 1720 cm^{-1} solid alane film absorption.[1,2] Hence, the alane oligomers on Al(111) are the next thing to solid alane.

Matrix Shifts. Table 5 compares frequencies for aluminum hydrides in neon, p-H_2, and n-H_2 solid hosts and shows that p-H_2 values fall between the neon and n-H_2 observations for both blue and red shifts. Note that the neon matrix DA absorptions are 1.5 and 2.7 cm^{-1} high for Al−H_2 stretching modes, 3.4 and 8.8 cm^{-1} low for Al−H−Al stretching modes, and all are within 2.9 cm^{-1} for the bending modes compared to n-H_2 matrix values. We expect more perturbation of the bridge modes by the hydrogen matrix host. It is very interesting to note that the DA fundamentals[2] in solid p-H_2 are intermediate between the neon and n-H_2 values, which is also the relationship found for AlH, AlH_2, and AlH_3 fundamentals. Hence n-H_2 perturbs the frequencies slightly more away from the neon values than p-H_2. How do solid p-H_2 and n-H_2 perturb the aluminum hydride frequencies progressively more? The hcp lattice parameter for n-H_2 is slightly shorter (3.769 Å) than that for p-H_2 (3.789 Å).[33,36,37] This means that 12 nearest-neighbor H_2 molecules will be 0.02 Å closer to the guest molecule and a stronger guest−host interaction will result in solid n-H_2. Another difference between the hydrogen solids is that the normal sample contains 3/4 of the molecules in the $J = 1$ rotational state, which have an anisotropic charge distribution, whereas in the para solid all molecules are in the $J = 0$ rotational state and are isotropic.[33] Hence stronger interactions will result with o-H_2 in the n-H_2 solid.

AlH in Solid Hydrogen. Several more considerations can be offered for AlH, the only aluminum hydride characterized in the gas phase.[16,21,38] The fundamental frequency in the gas phase is 1624.4 cm^{-1}, which red shifts to 1610.8 cm^{-1} in neon, to 1606.0 cm^{-1} in solid p-H_2, and to 1598.7 cm^{-1} in solid n-H_2. Vibrational constants $\omega_e = 1662.7$ and $\omega_e x_e = 28.4$ cm^{-1} can be calculated from the solid p-H_2 observations, which are intermediate between the gas phase (1682.6, 29.1 cm^{-1}) and n-H_2 (1654.7, 28.0 cm^{-1}) values.[2] In addition two sharp 1618.4, 1606.0 cm^{-1} and 1610.7, 1598.7 cm^{-1} bands for AlH in the two hydrogen solids and 1169.6, 1163.1 cm^{-1} for AlD in solid deuterium are observed.

It is much easier to document rotation of a stable molecule like HCl in solid matrices[39] than a transient molecule like AlH, which is prepared in limited quantity. The strong 1598.7 cm^{-1} band increases on 6 K annealing while the 1610.7 cm^{-1} band decreases, and this effect reverses on $\lambda > 380$ nm irradiation. The 1598.7 cm^{-1} band between 1624.4 cm^{-1} gas phase and 1590.7 cm^{-1} argon matrix fundamentals is clearly due to AlH. The growth of 1598.7 cm^{-1} at the expense of 1610.7 cm^{-1} absorption on annealing suggests an $AlH(H_2)_n$ complex for the former and possibly a smaller $AlH(H_2)_n$ complex for the latter. Irradiation (380 nm) then converts $AlH(H_2)_n$ to AlH_3 or the smaller complex AlH in the solid matrix.

This proposal of a $AlH(H_2)_n$ complex is supported by MP2 calculations. Although interaction of H_2 with the metal center in AlH is repulsive, we find weak bonding at the hydrogen site for a collinear complex presumably owing to the metal hydride polarity of AlH. Hence AlH does not function as a Lewis acid[40] like AlH_3 does in the formation of $(H_2)AlH_3$, and coordination of dihydrogen involves the hydride center. The frequency shifts calculated for AlH and H_2 in the complex are 0.5 and 18 cm^{-1}, respectively.

$$AlH + H_2 \rightarrow Al^{\delta+} - H^{\delta-} \text{ - - - } H-H \qquad [\Delta E = -1 \text{ kcal/mol}] \quad (9)$$

Formation of Charged Species. The laser-ablation process produces some Al^+ and e^-, which are incorporated into the deposited sample.[28,29] In addition, 193 nm irradiation increases the sharp 2959.4 cm^{-1} and the broad 2870 cm^{-1} absorptions (Figure 3) in the more rigid solid deuterium. The resonance absorptions of Al blue shift in solid matrices,[31] which allows ionization of Al in solid H_2 at 193 nm. Accordingly, the 4108.7 cm^{-1} cm^{-1} band is due to the H−H ligand vibration in the $Al^+(H_2)_n$ complex and the 3972 cm^{-1} band arises from the hydride complex $(H^-)(H_2)_n$. It is noteworthy that hydrogen atoms are abundant in these experiments for electron capture and subsequent formation of the hydride anion complex, reaction 10. Further evidence for the latter includes replacement by a 4067 cm^{-1} band upon doping with CCl_4 to in effect substitute H^- with Cl^-.[20] Apparently the rigid solid deuterium matrix is able to trap the charged species formed by 193 nm irradiation. The major Al^+ reaction here forms $Al^+(H_2)$; however, electron capture by $Al^+(H_2)$ during condensation will lead straightaway to AlH_2 from the insertion by excited Al atom,[13,30b] and such is probably the fate of most of the $Al^+(H_2)$ in these experiments. A similar 4115.5 cm^{-1} absorption has been observed in solid p-H_2 from laser-ablated aluminum and attributed to a positively charged species in part owing to its elimination when magnets are placed around the ablated material beam.[41]

$$H^- + nH_2 \rightarrow H^-(H_2)_n \quad (10)$$

$$Al^+ + H_2 \rightarrow Al^+(H_2) \quad (\Delta E = -1 \text{ kcal/mol, MP2}) \quad (11)$$

The identification of the sharp 4108.7 [2959.4] cm^{-1} bands (ratio 1.3884) as $Al^+(H_2)_n[Al^+(D_2)_n]$ complexes derives support from MP2 calculations. The side-bound complex $Al^+(H_2)$ is the stable isomer,[24,25] and MP2 calculations (Table 7) predict a 1 kcal/mol binding energy reaction 11, and 61 cm^{-1} red shift in the H−H stretching fundamental for $Al^+(H_2)$, which is in reasonable agreement with the 44 cm^{-1} observed shift for $Al^+(H_2)_n$. Further coordination of $Al^+(H_2)$ to $Al^+(H_2)_n$ in the hydrogen matrix is inevitable. In addition, the Ga^+ counterparts are observed at 4108.9 [2960.4] cm^{-1} (ratio 1.3880),[23] and MP2 calculations predict a 1.0 cm^{-1} higher frequency as compared to the 0.2 cm^{-1} higher value observed for $Ga^+(H_2)_n$. Finally, one can see that the bonding for Al^+, Al, and Al^- with H_2 are different; Al^+ forms the $Al^+(H_2)$ complex and not the insertion product like AlH_2, and AlH_2^- is extremely reactive in favor of the stable AlH_4^- alanate.

Another reaction for H^- in these experiments is with the strong Lewis acid AlH_3, reaction 12. This highly exothermic reaction forms the stable tetrahydroaluminate anion, AlH_4^-. The failure to observe AlH_2^- suggests that the major route to AlH_4^- is exothermic reaction 12, although electron capture by the $(H_2)AlH_2$ complex observed here at 1824.8 and 1790.2 cm^{-1}, as

proposed by Manceron et al.,[7] contributes as well.

$$AlH_3 + H^- \rightarrow AlH_4^- \quad (\Delta E = -72 \text{ kcal/mol, B3LYP}) \quad (12)$$

Jena and Khanna have explored the geometries of AlH_n^- clusters using DFT, which underscores the stability of the AlH_4^- alanate.[42] The possible rotation of tetrahedral AlH_4^- in solid hydrogen must be considered following such observations for methane.[37,43] Unfortunately, the ν_4 region for AlH_4^- is complicated by $AlH_{2,3}$ absorption, and the only absorption observed cleanly in solid n-H_2 is the ν_3 band at 1638.1 cm^{-1}. The fact that this band is higher than the neon value at 1627.8 cm^{-1} suggests that the 1638.1 cm^{-1} absorption might be due to the R(0) band whereas the neon and argon matrix absorptions are due to nonrotating AlH_4^-.

Molecular species in these experiments also capture electrons. We find no evidence for AlH^-, which is computed to absorb very strongly in the 1400 cm^{-1} region (Table 6). The AlD_2^- anion is observed in solid D_2, and near-UV irradiation converts AlD_2^- to AlD_4^-. We also note that annealing to 7.8 K allows the analogue of reaction 12 to proceed in solid deuterium. If formed in solid H_2, AlH_2^- reacts spontaneously to AlH_4^-. In contrast, both GaH_2^- and GaH_4^- are observed in solid hydrogen.[23] Finally, the AlH_3^- radical, observed at 1701.6 cm^{-1} in solid hydrogen, photodetaches with $\lambda > 530$ nm light.

Acknowledgment. We gratefully acknowledge support for this work from N.S.F Grant CHE 00-78836 and helpful discussions with M. E. Fajardo.

Table Added in Proof:

Infrared Absorptions (cm^{-1}) Observed from Co-deposition of Laser-Ablated Al Atoms and with Hydrogen and Deuterium Samples at 3.8 K

p-H_2[a]	n-H_2	n-D_2	o-D_2[a]	identification
4115.5	4108.7	2959.4	2959.0	$Al^+(H_2)_n$
4069.3	4061.6	2919.6	2921.1	$(H_2)AlH_3$
1933.3	1932.3	1415.0	1415.5	DA
1928.5	1927.2	1413.4	1414.0	DA site
1915.8	1915.1	1402.9		DA
1910.1	1909.1	1401.0		DA site
1885.5	1883.7	1378.7	1380.7	AlH_3 (ν_3, e)
1840.5	1838.4	1346.1	1345.9	Al_2H_4
1837.9	1835.8			Al_2H_4
1826.7	1825.5	1306.4	1306.5	Al_2H_4
1822.2	1821.9	1337.2	1337.2	AlH_2 (ν_3, b_2)
1788.0	1787.8	1293.1	1293.1	AlH_2 (ν_1, a_1)
1631.9	1638.1	1183.2	1182.5	AlH_4^-
1618.2	1610.7	1169.6	1172.8	AlH site
1605.9	1598.7	1163.1	1163.9	AlH
		1050.0	1048.8	AlD_2^-
		1043.0	1041.8	AlD_2^-
1406.5	1408.1	1028.5	1028.1	DA
1265.2	1268.2	919.9	918.8	DA
	1156.1	852.0		Al_2H_2
835.2	835.6	607.5	607.1	DA
779.6	777.9	561.8	560.1	AlH_3 (ν_4, e)
769.7	770.5	568.2	567.7	AlH_4^-
	770.5	560.3		AlH_2
	747	563		Al_2H_4
709.2	711.3	522.0	521.5	AlH_3 (ν_2, a_2'')
703.6	702.4	510.6	510.6	DA
631.1	631.9	459.1	458.4	DA

[a] p-H_2 and o-D_2 enrichment are 99%.

References and Notes

(1) Andrews, L.; Wang, X. *Science* **2003**, *299*, 2049.
(2) Wang, X.; Andrews, L.; Tam, S.; DeRose, M. E.; Fajardo, M. *J. Am. Chem. Soc.* **2003**, *125*, 9218.
(3) Duke, B. J.; Liang, C.; Schaefer, H. F., III. *J. Am. Chem. Soc.* **1991**, *113*, 2884.
(4) Shen, M.; Liang, C.; Schaefer, H. F., III. *Chem. Phys.* **1993**, *171*, 325.
(5) Mitzel, N. W. *Angew. Chem.* **2003**, *42*, 3856.
(6) Cotton, F. A.; Wilkinson, G.; Murillo, C. A.; Bochmann, M. *Advanced Inorganic Chemistry*, 6th ed.; Wiley: New York, 1999.
(7) Pullumbi, P.; Bouteiller, Y.; Manceron, L. *J. Chem. Phys.* **1994**, *101*, 3610.
(8) Rao, B. K.; Jena, P.; Burkart, S.; Ganteför, G.; Seifert, G. *Phys. Rev. Lett.* **2001**, *86*, 692.
(9) Wang, X.; Andrews, L. *J. Phys. Chem. A* **2003**, *107*, 570.
(10) Wang, X.; Andrews, L. *J. Am. Chem. Soc.* **2003**, *125*, 6581.
(11) Legay-Sommaire, N.; Legay, F. *Chem. Phys. Lett.* **1993**, *207*, 123.
(12) Chertihin, G. V.; Andrews, L. *J. Phys. Chem.* **1993**, *97*, 10295.
(13) Pullumbi, P.; Mijoule, C.; Manceron, L.; Bouteiller, Y. *Chem. Phys.* **1994**, *185*, 13.
(14) Pullumbi, P.; Bouteiller, Y.; Manceron, L.; Mijoule, C. *Chem. Phys.* **1994**, *185*, 25.
(15) Kurth, F. A.; Eberlein, R. A.; Schnöckel, H.; Downs, A. J.; Pulham, C. R. *J. Chem. Soc. Chem. Commun.* **1993**, 1302.
(16) Huber, K. P.; Herzberg, G. *Constants of Diatomic Molecules*; Van Nostrand, Princeton, 1979.
(17) Liang, C.; Davy, R. D.; Schaeffer, H. F., III. *Chem. Phys. Lett.* **1989**, *159*, 393.
(18) Shen, M.; Schaefer, H. F., III. *J. Chem. Phys.* **1992**, *96*, 2868.
(19) Stephens, J. C.; Bolton, E. E.; Schaefer, H. F., III; Andrews, L. *J. Chem. Phys.* **1997**, *107*, 119.
(20) Wang, X.; Andrews, L. *J. Phys. Chem. A* **2004**, *108*, 1103.
(21) Zhu, Y. F.; Shehadeh, R.; Grant, E. R. *J. Chem. Phys.* **1992**, *97*, 883.
(22) Gush, H. P.; Hare, W. F. J.; Allin, E. F.; Welsh, H. L. *Can. J. Phys.* **1960**, *38*, 176.
(23) Wang, X.; Andrews, L. *J. Phys. Chem. A* **2003**, *107*, 11371 (Ga + H_2).
(24) Niu, J.; Rao, B. K.; Jena, P. *Phys. Rev. B* **1995**, *51*, 4475.
(25) Rasul, G.; Prakash, G. K. S.; Olah, G. A. *J. Phys. Chem. A* **2000**, *104*, 2284.
(26) Moore, C. E. Atomic Energy Levels, *Cir. Natl. Bur. Std.*, 467, Washington, DC, 1952.
(27) CRC Handbook, Line Spectra of the Elements, 66th ed.; Boca Raton, FL, 1985.
(28) Fajardo, M. E.; Macler, M.; Tam, S. *High Energy Density Matter Contractors Conference*, Boulder, CO, 1996.
(29) Kang, H.; Beauchamp, J. L. *J. Phys. Chem.* **1985**, *89*, 3364.
(30) (a) Abe, H.; Kolb, D. M. *Ber. Bunsen-Ges. Phys. Chem.* **1983**, *87*, 523. (b) Parnis, J. M.; Ozin, G. A. *J. Phys. Chem.* **1989**, *93*, 1204.
(31) (a) Ammeter J. H.; Schlosnagle, D. C. *J. Chem. Phys.* **1973**, *59*, 4784. (b) Douglas, M. A.; Hauge,. R. H.; Margrave, J. L. *J. Chem. Soc., Faraday Trans.* **1983**, *79*, 1533. (c) Grinter, R.; Singer, R. J. *Chem. Phys.* **1987**, *113*, 87. (d) Fajardo, M. E.; Tam, S.; Thompson, T. L.; Cordonnier, M. E. *Chem. Phys.* **1994**, *189*, 351.
(32) Andrews, L.; Wang, X. *J. Phys. Chem. A* **2002**, *106*, 7696.
(33) Silvera, I. F. *Rev. Mod. Phys.* **1980**, *52*, 393.
(34) Knight, L. B., Jr. Personal communications, 2003.
(35) Go, E. P.; Thuermer, K.; Reutt-Robey, J. E. *Surf. Sci.* **1999**, *437*, 377.
(36) Krupskii, I. N.; Prokhvatilov, A. I.; Shcherbakov, G. N. *Sov. J. Low Temp. Phys.* **1983**, *9*, 446.
(37) Krupskii, I. N.; Prokhvatilov, A. I.; Shcherbakov, G. N. *Sov. J. Low Temp. Phys.* **1983**, *9*, 42.
(38) Deutsch, J. L.; Neil, W. S.; Ramsay, D. A. *J. Mol. Spectrosc.* **1987**, *125*, 115.
(39) Anderson, D. T.; Hinde, R. J.; Tam, S.; Fajardo, M. E. *J. Chem. Phys.* **2002**, *116*, 594.
(40) See, for example, Gordon, J. D.; Voigt, A.; Macdonald, C. L. B.; Silverman, J. S.; Cowley, A. H. *J. Am. Chem. Soc.* **2000**, *122*, 950.
(41) Fajardo, M. E.; Tam, S. *J. Chem. Phys.* **1998**, *108*, 4237. Fajardo, M. E., personal communication, 2004.
(42) Jena, P.; Khanna, S. N. *Phys. Rev. Lett.*, in press.
(43) Tam, S.; Fajardo, M. E.; Katsuki, H.; Hoshina, H.; Wakabayashi, T.; Momose, T. *J. Chem. Phys.* **1999**, *111*, 4191.